# Evaluation of the electrochemical active surface area for carbon felt and nanostructured Ni coatings as electrocatalysts for hydrogen evolution reaction

Dmitry S. Dmitriev, Maksim I. Tenevich

Ioffe Institute, St. Petersburg, Russia

Corresponding author: Dmitry S. Dmitriev, elchemorg@gmail.com

ABSTRACT This study is devoted to the evaluation of electrochemical active surface area (ECSA) for carbon felt used in various fields of electrochemical technology. For the evaluation, we used techniques based on Faraday's law, the Randles–Sevcik equation and the calculation of the electric double layer capacitance in the electrolyte with different pH value. The measurement results are consistent with each other and for neutral, acidic and alkaline medium, the ECSA value are $20 - 30$, $30 - 40$ and $50 - 90$ $cm^2$ per 1 $cm^2$ of geometric surface, respectively. Based on the results, the synthesis of nanostructured nickel coatings on carbon felt with prior electrochemical activation was performed. The pre-treatment in 1M KOH vs 1 M $Na_2SO_4$ reduces the crystallite size from 26 to 15 nm and increases the ECSA from 133 to 700 $cm^2$ per 1 $cm^2$ of geometric surface. These changes cause an improvement in other electrocatalytic features for hydrogen evolution reaction.

## 1. Introduction

The development of new electrode materials is carried out in all fields of electrochemical technology from electro-catalysts of water splitting reactions to chemical current sources and supercapacitors. Currently, the use of porous carbon materials (fibers, felt) as a substrate is popular. Carbon felt is a polyacrylonitrile (PAN) or viscose fiber that has been needle-punched to form a structure and carbonized at $1200 - 1600$ °C or graphitized at $2000 - 2600$ °C [1]. Carbon felt is widely used in redox-flow batteries [2–7], lithium-, sodium- and zinc-ion batteries [8–15], as well as in supercapaci-tors [16–21] and alternative energy storage and generation technologies [22–25]. Mingxing Wu et al. have shown that the inclusion of cobalt particles in carbon fibers [13] increases the efficiency of the zinc-air battery, and boron doping [16] improves their capacitive properties when used as supercapacitor electrodes. In addition, carbon fibers are used in the synthesis of electrocatalysts for the reaction of hydrogen, oxygen production and the Fenton process [26–34]. Paper [30] reports on the synthesis of rhenium disulfide nanosheets on the carbon fiber surface as an effective electrocatalyst of the hydrogen evolution reaction (HER) with overpotential values of 69 mV@ 10 mA·cm$^{-2}$ and Tafel slope of 90 mV·dec$^{-1}$.

Unlike a metal substrate, carbon materials are economically and environmentally beneficial, more resource-intensive and can be removed thermally in the next, i.e. they are able to perform the role of templates [35–39]. This makes it possible to significantly increase the electrochemically active surface area of electrode materials, which has a positive effect on their functional features. Paweł Jakobczyk et al. [38] have shown that thermal and chemical modification of the carbon felt surface improves its catalytic properties in the acetaminophen degradation reaction. The authors of [26] declare the successful use of modified carbon felt as a cathode in the Fenton process for the removal of tetracycline. Modification was carried out together by chemical and thermal methods. This allowed one to reduce the relative concentration of tetracycline during the Fenton process by two times. In paper [36], we previously showed that the use of carbon felt as a template makes it possible to obtain copper microtubes with a lower overpotential of HER.

However, the authors using carbon felt in their research are often limited to their geometric (visible) surface area ($S_{geo}$, cm$^2$) or report the surface area of the final material after activation or modification of the fiber. In the datasheet of carbon felt from various manufacturers, approximate values of the surface area are given, usually estimated by the method of low-temperature adsorption calculated using the Brunauer–Emmett–Teller (BET) method [40–48]. These values do not always correspond to the electrochemical active surface area obtained by electrochemical methods [1, 49–51]. The value of the specific surface area ($A_m$, m$^2$g$^{-1}$) obtained by the BET method varies from 0.12 to 8 m$^2$g$^{-1}$. The most commonly mentioned value is $1.1 - 1.3$ m$^2$g$^{-1}$. The results of ECSA obtained by electrochemical methods (from the

Randles–Sevcik and Cottrell equations) are also different and are given by the authors without taking into account mass, geometric surface or volume. On average, for a sample with a visible surface of 10 cm$^2$, the ECSA value is 40 – 50 cm$^2$.

In this paper, we have tried to evaluate the ECSA by three different electrochemical techniques: 1) on the basis of Faraday's law, measuring the thickness of nickel coatings obtained during coulostatic and galvanostatic modes of electroplating; 2) from calculating the value of electric double layer capacitance (EDLC), as the most common method due to its simplicity and clarity of the values obtained; and 3) from the Randles–Sevcik equation for single-electron redox process involving potassium ferrocyanide.

Based on the results, the synthesis of nanostructured nickel coatings on carbon felt with electrochemical surface pre-treatment in a neutral and alkaline medium was carried out. The electrocatalytic activity of these coatings was evaluated and the ECSA value was measured.

## 2. Experimental detail

### 2.1. Materials

The following materials and reagents were used in the study:

Carbon Felt (CF) (Beijing Great Wall Co., Ltd.)), Nickel sulfate ($NiSO_4 \times 7H_2O$), Sodium sulfate ($Na_2SO_4 \times 10H_2O$), Boric acid ($H_3BO_3$), Potassium chloride (KCl), Sulfuric acid ($H_2SO_4$), Potassium hydroxide (KOH), Potassium ferrocyanide ($K_4Fe(CN)_6 \times 3H_2O$) from Nevareaktiv.

Platinum foil (Pt, 99.999 %), Copper wire (Cu, 99.999 %), Nickel plates (Ni, 99.99 %), Distilled water ($\Omega = 18$MOhm·cm) were also used in this work.

### 2.2. Experimental and measurement conditions

*2.2.1. Nickel electroplating.* Carbon felt ($1.25 \times 0.5 \times 0.5$ cm) with copper wire ($d = 0.4$ mm) as a collector was used for nickel electroplating. The geometric surface area was $S_{geo} = 3$ cm$^2$. Electroplating was carried out in Watts electrolyte (Table 1) at the room temperature with a magnetic stirrer. Nickel plates with a working surface area of $S_a = 10$ cm$^2$ were used as anodes. The experiment was carried out in two series: with a fixed current value (30 mA) and with a constant amount of electricity (30 mA·h). In the both series, the process was performed for 0.5, 1, 2 hours.

TABLE 1. Electrolyte composition and nickel electroplating mode

| Component | Concentration g/L |
|---|---|
| $NiSO_4 \times 7H_2O$ | 75 |
| $Na_2SO_4 \times 10H_2O$ | 50 |
| $H_3BO_3$ | 25 |
| KCl | 10 |

pH = $5.6 \pm 0.1$; $T = 25$ °C;
1st series: $I = 30$ mA=const; $t = 0.5, 1, 2$ h;
2nd series: $Q = It = 30$ mA·h (15 mA·2 h, 30 mA·1 h, 60 mA·0.5 h)

Before electrolysis, carbon felt was treated with ultrasound in ethanol for 10 minutes to degreasing, degassing and improving the wettability of surface. After electroplating, the samples were rinsed in warm (60 °C) and room (25 °C) distillate and dried at 100 °C for 1 hour.

Weighing of samples (carbon felt + copper wire) for gravimetric analysis was performed before ultrasonic treatment ($m_0$) and after drying ($m_1$). The thickness of the synthesized coatings was measured using a scanning electron microscope TESCAN SEM with the VEGA 3 SBH microanalyzer.

In the second part of the study, nickel electrodeposition was performed with electrochemical pre-treatment of carbon felt in solutions of 1M $Na_2SO_4$ and 1 M KOH for 10 min at a current density of 10 mA·cm$^{-2}$. Next, the samples were rinsed in distillate and nickel electrodeposition was performed at a current density of 10 mA·cm$^{-2}$ for 1 hour. After that, the samples were rinsed in warm and room distillate and dried for 1 hour at 100 °C. The synthesized coatings were labeled Ni@CF-$Na_2SO_4$ and Ni@CF-KOH, respectively.

*2.2.2. Voltammetric techniques.* Cyclic voltammetry (CVA) was executed in a three-electrode cell using a potentiostat-galvanostat ELINS P-45X equipped with a frequency response analyzer module FRA-24M. During the measurements, carbon felt samples with dimensions of $2.75 \times 0.5 \times 0.5$ (cm) ($S_{geo} = 6$ cm$^2$) were used, mounted on a JJ110 sample holder with a platinum plate as a collector. The platinum plate ($S = 1$ cm$^2$) and Ag/AgCl ($E^0_{Ag/AgCl} = 0.194$ V, 3 M KCl) were counter and reference electrodes, respectively. The obtained polarization curves were converted to the scale of the normal hydrogen electrode (NHE):

$$E_{NHE} = E_{\text{Ag/AgCl}} + E^0_{\text{Ag/AgCl}}. \tag{1}$$

When measuring the capacitance of electric double layer, solutions of $H_2SO_4$, $Na_2SO_4$ and KOH with a concentration of 1 M were used as electrolytes. The mass of the sample was $m = 70$ mg. Previously, the sample was treated with ultrasound in ethanol for 10 minutes to degreasing, degassing and improving the wettability of surface. The solution was stirred using a magnetic stirrer. Measurements were performed from the open circuit potential (OCP) to the potential corresponding to overpotential of HER $dE_{HER} = -400$ mV. Scanning rates ($v$) were 10, 20, 40, 60, 80, 100 mV·s$^{-1}$.

To study the redox reaction

$$[\text{Fe(CN)}_6]^{4-} - e \Leftrightarrow [\text{Fe(CN)}_6]^{3-}$$

a solution of 0.005 M $K_4Fe(CN)_6$ + 0.1 M KCl was used as the electrolyte. The mass of the sample in this test was $m = 78$ mg. Measurements were carried out starting from the OCP to the anode side. The range of scanning potentials was from $-200$ to 800 mV vs Ag/AgCl. Scanning rates ($v$) were 10, 20, 40, 60, 80, 100 mV·s$^{-1}$.

*2.2.3. Characterization of pre-treated nickel coatings.* The structure and morphology of the synthesized samples were studied using a scanning electron microscope TESCAN SEM with the VEGA 3 SBH microanalyzer (EDX-mapping). XRD analysis was performed on a Rigaku SmartLab III diffractometer (CuKa radiation, $\lambda = 0.15405$ nm).

The electrocatalytic properties of Ni@CF-Na$_2$SO$_4$ and Ni@CF-KOH were evaluated by the CVA with the determination of Tafel slope, ECSA and the turnover frequency (TOF). The methodology and equipment used are similar to paragraph 2.2.2.

## 2.3. Calculation methods

*2.3.1. The ECSA from Faraday's Law ($A_{ED}$).* The calculation of the ECSA value from the thickness of electrodeposited nickel was carried out in two steps. Initially, a selection of values was collected from the coating thicknesses in the SEM images (Fig. A1, Appendix). The average number of values in the selection for each sample was 35. Further, the values were statistically processed to determine the absolute and relative ($\varepsilon$) errors (probability $P = 0.99$). At the second step, the values obtained for the samples synthesized in the coulostatic mode were compared with each other, and for the samples electrodeposited in the galvanostatic mode, a graphical dependence of the coating thickness on the electrolysis time was constructed.

According to Faraday's law

$$m = q_{Ni} \cdot Q \cdot FE, \tag{2}$$

$$\rho A_w H = q_{Ni} \cdot It \cdot FE, \tag{3}$$

$$H(t) = \frac{q_{Ni} \cdot I \cdot FE}{\rho A_w} \cdot t, \tag{4}$$

$$H(t) = n \cdot t; \quad n = \frac{q_{Ni} \cdot I \cdot FE}{\rho A_w}, \tag{5}$$

where $m$ is the mass of deposited nickel (g), $q_{Ni}$ is the electrochemical equivalent of the nickel plating process (gA$^{-1}$h$^{-1}$), $Q$ is the amount of electricity (C), FE is the Faraday efficiency, $p_{Ni}$ is the nickel density (gcm$^{-3}$), $A_w$ is the working surface area (cm$^2$), $H$ is the coating thickness (cm), $I$ is the current (A), $t$ is the electrolysis time (h). Hence the working surface $A_w$ is as follows

$$A_w = \frac{q \cdot I \cdot FE}{\rho \cdot n}, \tag{6}$$

and the specific value of ECSA:

$$A_{ED} = \frac{A_w}{S_{geo}}. \tag{7}$$

*2.3.2. The ECSA from EDLC value ($A_{DL}$).* To calculate the EDLC, a graph was plotted in the coordinates $\Delta_j = f(v)$, where

$$\Delta j = \frac{|j_a + j_c|}{2}, \tag{8}$$

$\Delta_j$ is the arithmetic mean of the anode ($j_a$) and cathode ($j_c$) current densities (mA·cm$^{-2}$).

The EDLC ($C_{dl}$) was obtained from the slope of the approximation line. Further, the specific value of ECSA was calculated according to the expression

$$A_{DL} = \frac{C_{dl}}{C^*}, \tag{9}$$

where $C^* = 0.08$ mF·cm$^{-2}$ is the specific value of the capacitance on a porous, highly active and inhomogeneous surface.

*2.3.3. The ECSA from Randles–Sevcik equation ($A_{RS}$).* To determine the specific value of ECSA during CVA in a solution of 0.005 M $K_4Fe(CN)_6$ + 0.1 M KCl, a graphical dependence $j_{pa,geo} - (v)^{0.5}$ was constructed, according to the Randles–Sevcik equation

$$j_{pa,geo} = 2.69 \times 10^5 A_{RS} C_{ox} n^{1.5} D^{0.5} v^{0.5}, \tag{10}$$

$$j_{pa,geo} = k \cdot v^{0.5}; \quad k = 2.69 \times 10^5 A_{RS} C_{ox} n^{1.5} D^{0.5}, \tag{11}$$

where $j_{pa,geo}$ is anodic peak current density (per geometric surface) (A·cm$^{-2}$), $2.69 \cdot 10^5$ is the constant of the Randles–Sevcik equation (C·mole$^{-1}$·V$^{-0.5}$), $A_{RS}$ is the electrochemical active surface area (cm$^2$ per 1 cm$^2$ geometric), $C_{ox}$ is the concentration of the oxidized form (mole·cm$^{-3}$), $n$ is the number of electrons involved in the reaction, $D$ is the diffusion coefficient (cm$^2$s$^{-1}$), $v$ is the scanning rate (V·s$^{-1}$).

From the slope value ($k$) of the linear approximation, the specific value of ECSA was calculated by the following expression

$$A_{RS} = \frac{k}{2.69 \cdot 10^5 \cdot C_{ox} \cdot n^{1.5} \cdot D^{0.5}}. \tag{12}$$

## 3. Results and discussion

### 3.1. Evaluation of the ECSA from coating thickness by Faraday's law

Table 2 presents the results of gravimetric analysis for carbon felt samples and the average Faraday efficiency ($\overline{FE}$) for the nickel electrodeposition process.

TABLE 2. Results of nickel electroplating

| Sample | Current, mA | Time, h | $m_0$, mg | $m_1$, mg | $\Delta m$, mg | $\Delta m_{teo}$, mg | FE | |
|--------|-------------|---------|-----------|-----------|----------------|----------------------|------|---|
| Ni-30-0.5 | 30 | 0.5 | 106.3 | 121.8 | 15.5 | 16.4 | 0.94 | |
| Ni-30-1 | 30 | 1 | 104.4 | 134.5 | 30.1 | 32.9 | 0.92 | |
| Ni-30-2 | 30 | 2 | 108.0 | 172.0 | 64.0 | 65.7 | 0.97 | $\overline{FE} = 0.95$ |
| Ni-15-2 | 15 | 2 | 106.6 | 137.6 | 31.0 | 32.9 | 0.94 | |
| Ni-60-0.5 | 60 | 0.5 | 102.7 | 134.8 | 32.1 | 32.9 | 0.98 | |

It can be noted that the process proceeds with high efficiency (95 %), the remaining 5 % of electricity is spent to the hydrogen evolution reaction on the forming coating surface. Fig. 1 shows the results of measuring the thickness of the coating during coulostatic and galvanostatic electrodeposition of nickel on carbon felt.

In coulostatic electrolysis, the thickness of the nickel coating is $H_1 = 0.57 \pm 0.02$ microns ($\varepsilon = 3.5$ %). When passing the same amount of electricity in galvanostatic mode, the nickel coating has a thickness of $H_2 = 0.54 \pm 0.02$ microns ($\varepsilon = 2.9$ %). The working surface areas, in this case, are equal

$$A_{w1} = \frac{q \cdot Q \cdot \overline{FE}}{\rho_{Ni} \cdot H_1} = \frac{1.095 \cdot 0.03 \cdot 0.95}{8.9 \cdot 0.57 \cdot 10^{-4}} = 62.2 \text{ cm}^2, \quad \Delta A_1 = \pm(62.2 \cdot 0.035) = \pm 2.2 \text{ cm}^2,$$
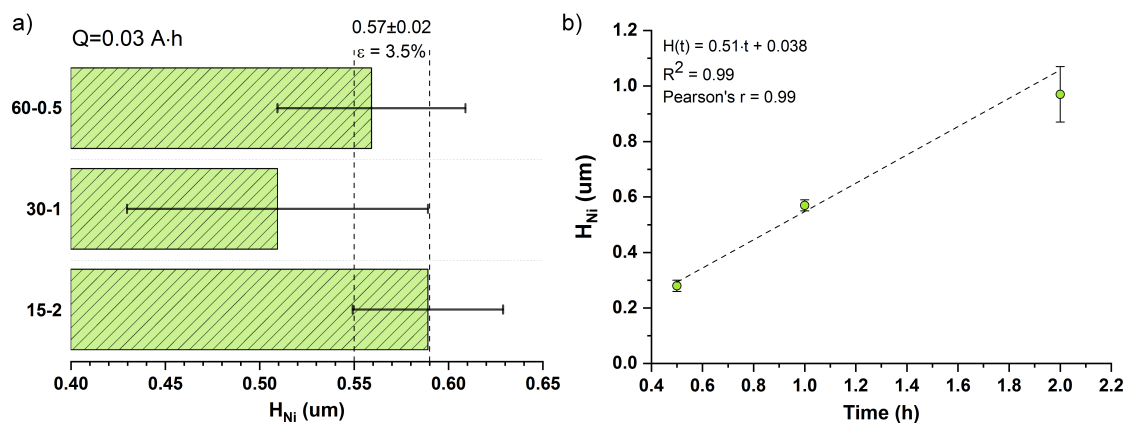


FIG. 1. Results of electroplating nickel in coulostatic (a) and galvanostatic (b) modes

$$A_{w2} = \frac{q \cdot Q \cdot \overline{FE}}{\rho_{Ni} \cdot H_2} = \frac{1.095 \cdot 0.03 \cdot 0.95}{8.9 \cdot 0.54 \cdot 10^{-4}} = 65.6 \text{ cm}^2, \quad \Delta A_2 = \pm(65.6 \cdot 0.029) = \pm 1.9 \text{ cm}^2.$$

These values are overlapped in the region $A_w = (64.05 \pm 0.35)$ cm$^2$, and the specific ECSA value of the carbon felt during electrodeposition is

$$A_{ED} = \frac{A_w}{S_{geo}} = \frac{64.05}{3} = 21.35 \text{ cm}^2 \text{ per } 1 \text{ cm}^2 \text{ geometric.}$$

## 3.2. Evaluation of the ECSA from double layer capacitance

Determination of the ECSA from the value of EDL capacitance is one of classical methods. Fig. 2(a) shows the linear approximations in the coordinates $\Delta j - v$. The slope coefficient of these lines is numerically equal to the capacitance of double layer. Using expression (9), ECSA values for carbon felt in acidic, neutral and alkaline environments were calculated. From the presented histograms (Fig. 2(b)), we can conclude about the advantage of alkaline solutions when using carbon felt as an electrode material. The ECSA value in alkaline, acidic and neutral media is 95, 34.3 and 26.8 cm$^2$ per 1 cm$^2$ geometric. Presumably, this result is caused by the greater lyophilicity of the carbon filament in an alkaline medium compared to acidic and neutral media.
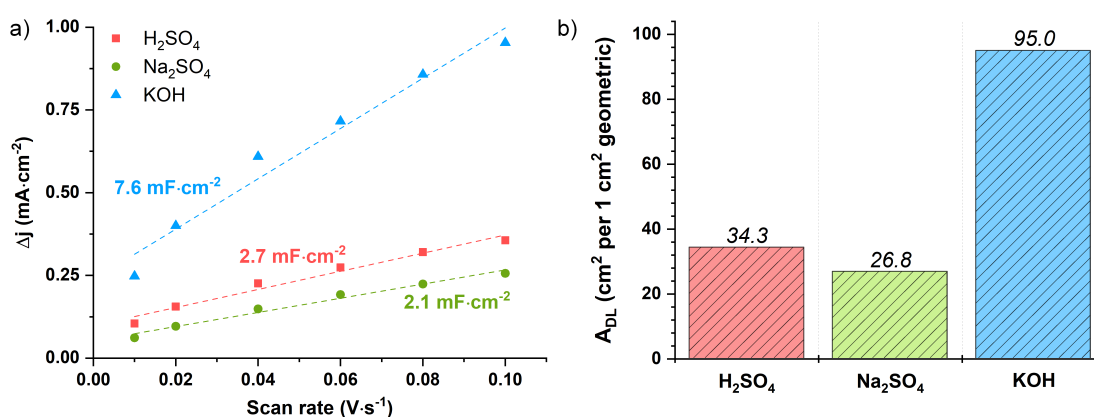


FIG. 2. Capacitance plot (a) and values of ECSA (b) for carbon felt in different electrolyte

It is worth noting that when using an acid solution as an electrolyte on the CVA curves (Fig. A2, Appendix), an anode peak is observed at a potential of $E = 0.23$ V vs NHE, which corresponds to the oxidation of ethanol used in pre-preparation.

## 3.3. Evaluation of the ECSA from Randles–Sevcik equation

The results of processing CVA curves are shown in Fig. 3.

It can be seen from Fig. 3(a) that with increasing scanning rate, the process taking place on the electrode under study becomes less reversible or quasi-reversible. The probable cause may be diffusion control due to the porosity of the electrode, which makes it difficult for natural convection and the movement of reagents from the reaction zone into the bulk of the solution. This is confirmed by the slope of the linear approximation in $\log(j_{geo}) - \log(v)$ coordinates
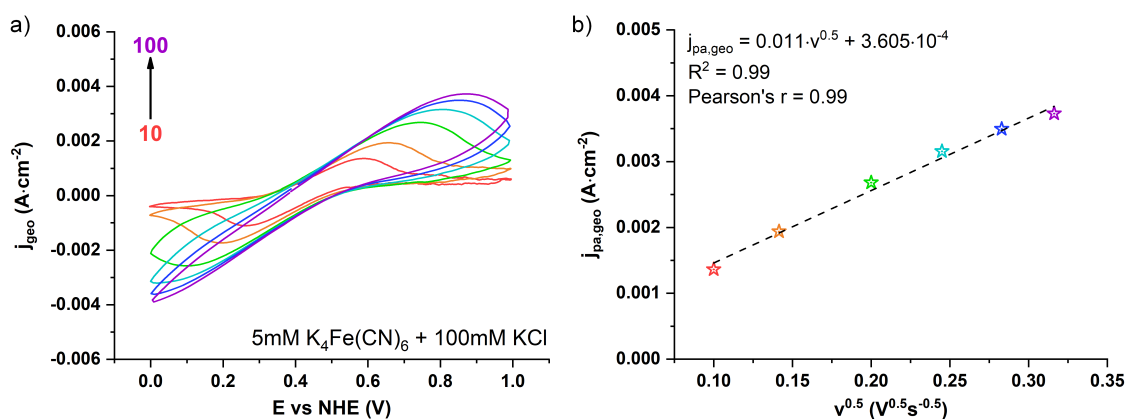


FIG. 3. CVA curves of $[Fe(CN)_6]^{4-}/[Fe(CN)_6]^{3-}$ process (a) and the Randles–Sevcik plot (b)

(Fig. A3(a), Appendix) equal to $m = 0.44$. For reactions with diffusion limitations, it is as follows: $m = 0.4 \pm 0.1$. From the linear approximation in the coordinates $j_{pa,geo} - v^{0.5}$, the slope was determined for further calculation of the surface area (Fig. 3(b)). The ECSA value from the Randles–Sevcik equation is equal to

$$A_{RS} = \frac{0.011}{2.69 \cdot 10^5 \cdot 3.1 \cdot 10^{-7} \cdot 1^{1.5} \cdot (6.5 \cdot 10^{-6})^{0.5}} = 51.6 \text{ cm}^2 \text{ per 1 cm}^2 \text{ geometric.}$$

The calculation used the effective concentration of the oxidized form obtained by integrating the polarization curve at the lowest scanning rate in I–t coordinates (Fig. A3(b), Appendix). As a result of diffusion limitations, the pH of the near-electrode region shifts to a slightly-alkaline range, which gives a higher ECSA value. This value is consistent with the one previously obtained in work [1].

### 3.4. Comparison of the evaluation results and the ECSA value for carbon felt

Table 3 summarizes the evaluation of ECSA values obtained by various electrochemical techniques.

TABLE 3. The ECSA values of carbon felt by various electrochemical techniques

| Technique | ECSA, cm$^2$ per 1 cm$^2$ geometric |
|---|---|
| Faraday's law | 21.4 |
| Double layer capacitance | 34.3 (pH $<$ 7) <br> 26.8 (pH $\approx$ 7) <br> 95.0 (pH $>$ 7) |
| Randles–Sevcik equation | 51.6 |

As can be seen, the specific value of ECSA for carbon felt lies in the range from 20 to 100 cm$^2$ per 1 cm$^2$ geometric surface. The ECSA significantly depends on the pH electrolyte used, and for acidic and neutral media, its range of values is $20 - 40$ cm$^2$ per 1 cm$^2$ geometric surface. In an alkaline media, activation of the surface is observed [32], as a result of which the area increases at least $8 - 10$ times. Comparing the results of ECSA with the average values of the specific surface area for carbon felt measured by the BET method, it can be determined that the ECSA in acidic and neutral media is $0.1 - 0.3$ m$^2$g$^{-1}$, and in alkaline it is $0.4 - 0.8$ m$^2$g$^{-1}$. This is $1.5 - 4$ times lower than the average value $S_{BET} = 1.2$ m$^2$g$^{-1}$. This difference is, among other things, due to the low lyophilicity of carbon materials in aqueous electrolytes, as a result of which it is recommended to use surfactants, or to activate the surface by chemical and thermal methods.

### 3.5. Effect of carbon felt pre-treatment on electrocatalytic features of nanostructured nickel coatings

Figure 4(a,b) shows the SEM results with mapping. It can be seen from the SEM images that the morphology of coating with pre-treatment in an alkaline solution differs significantly from a similar process in a neutral medium. The Ni@CF-KOH coating is not smooth, unlike Ni@CF-Na$_2$SO$_4$, has a distinct defect in the form of dendrites on surface.

The results of XRD analysis (Fig. 4(c)) demonstrate the presence of a carbon felt phase at $20 - 30$ degrees and peaks corresponding to ICSD card No. 426960, which describes the cubic modification of nickel. According to calculations, the observed broadening for the characteristic nickel peaks (Fig. 4(d)) indicates a decrease in the crystallite sizes from 26.5 to 15.1 nm.

The results of electrocatalytic measurements for synthesized coatings are shown in Fig. 5. When using as an electrolyte for the pre-treatment of 1 M KOH instead 1 M Na$_2$SO$_4$, an improvement in the main electrocatalytic features of HER is observed.

Figure 5(a,b) demonstrates that the overpotential value shifts from $-210$ to $-120$ mV. At the same time, the absolute value of Tafel slope decreases. The value greater than 120 mVdec$^{-1}$ indicates a reaction mechanism with the presence of diffusion limitations, which corresponds to the Volmer–Tafel model:

$$\text{M}^* + \text{H}_2\text{O} + e \leftrightarrow \text{MH}_{\text{ads}} + \text{OH}^- \qquad \text{(Volmer step)}$$

$$2\text{MH}_{\text{ads}} \leftrightarrow \text{H}_2 + 2\text{M}^* \qquad \text{(Tafel step)}$$
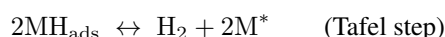
The ECSA measurement shows a sharp increase in both the EDLC and the surface area value (Figs. 5(c) and A4). For Ni@CF-Na$_2$SO$_4$ and Ni@CF-KOH, the ECSA value is 133 and 700 cm$^2$ per 1 cm$^2$ geometric surface, respectively. There was also an improvement in the coating efficiency from the results of TOF-test (Fig. 5(d)).

It can be seen that the electrochemical activation of carbon felt in an alkaline solution allows obtaining a more catalytically active surface both in terms of the value of surface area and improving kinetic parameters. All this results in a synergistic effect expressed by an increase in the total number of molecules transformations per unit surface per unit time.

*D.S. Dmitriev, M.I. Tenevich*
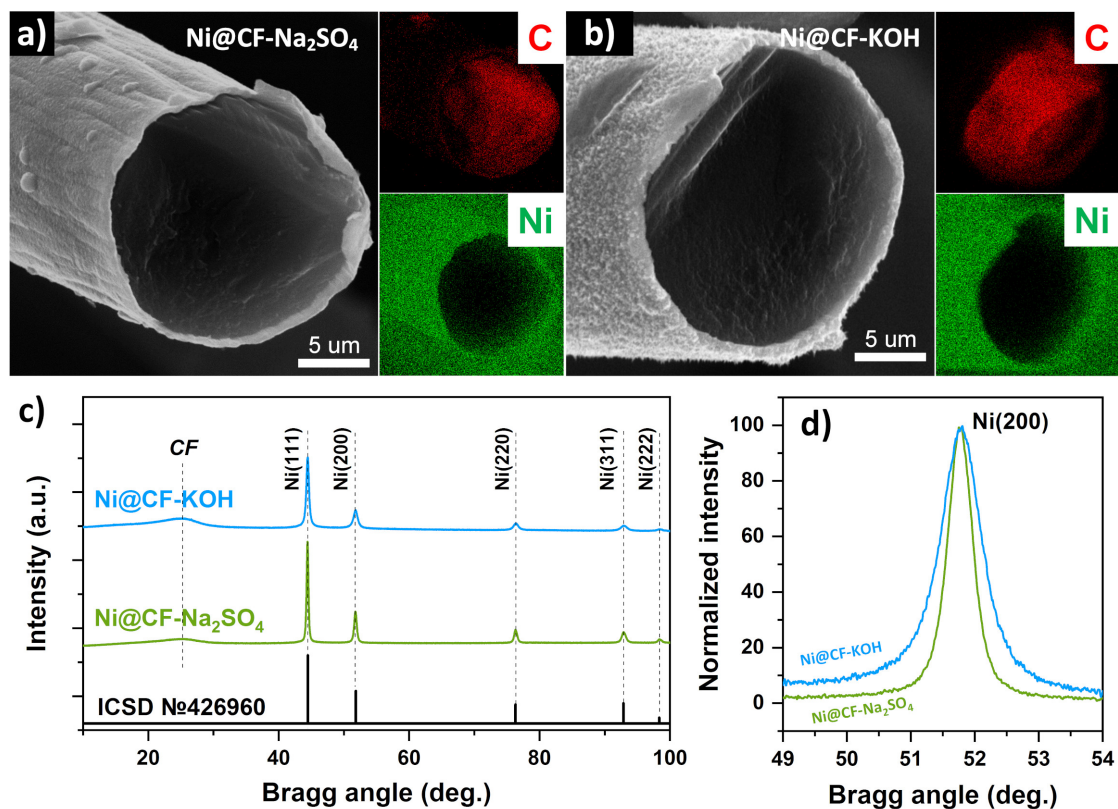


FIG. 4. SEM images (a, b) and XRD patterns (c, d) for synthesized samples
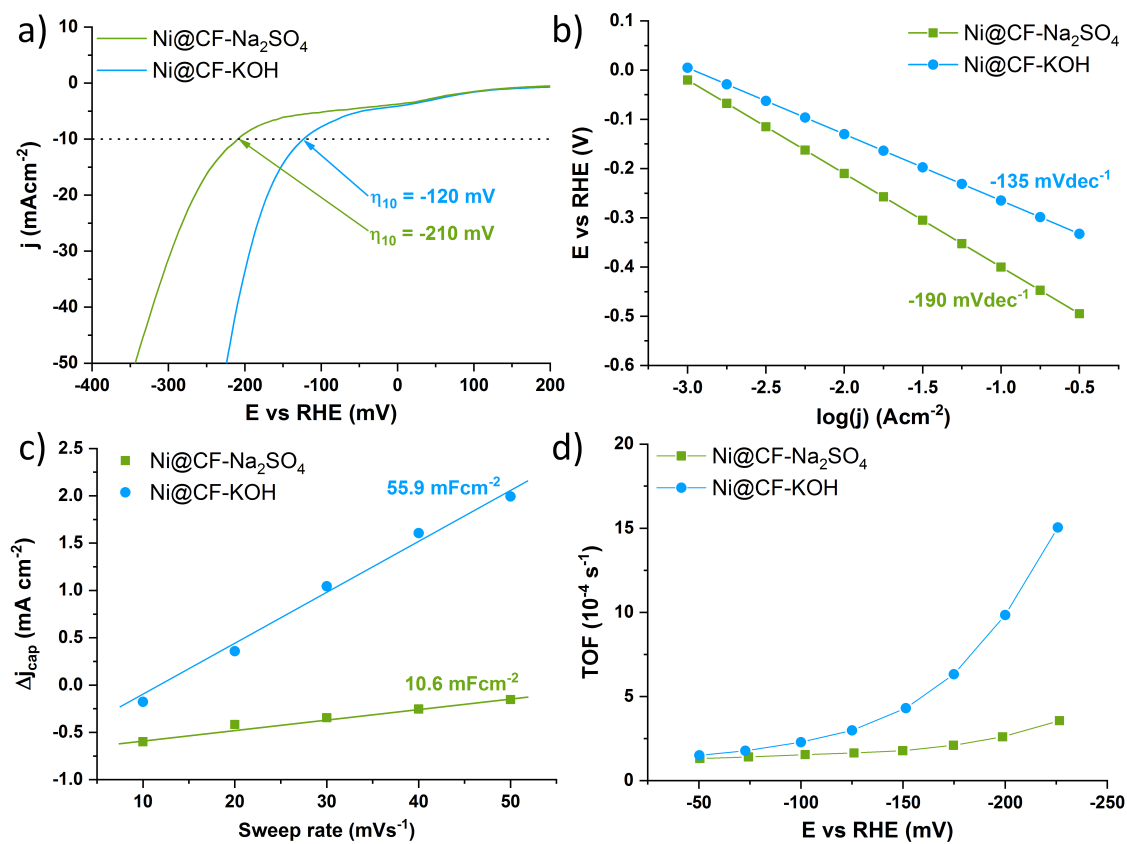


FIG. 5. LSV curves (a), Tafel plot (b), capacitance plot (c) and TOF result (d) for Ni@CF-Na$_2$SO$_4$ and Ni@CF-KOH

## 4. Conclusion

Based on the study results, it can be concluded that

 (i) The evaluation of ECSA by various techniques gives convergent results within 1 order of magnitude when using electrolytes with the same pH value.

 (ii) For a neutral medium, the ECSA of carbon felt can be assumed to be $20 - 30$ cm$^2$ per 1 cm$^2$ geometric surface. For acidic and alkaline media, the ECSA value is $30 - 40$ cm$^2$ and $50 - 100$ cm$^2$ per 1 cm$^2$ geometric surface, respectively.

 (iii) When estimating the ECSA from the Randles–Sevcik equation, diffusion limitations are observed in the redox process. This shifts the pH of near-electrode layer to a slightly-alkaline range and overestimates the ECSA value of carbon felt.

 (iv) It is shown that the electrochemical activation of carbon felt in neutral and alkaline solutions allows the synthesis of nanostructured nickel coatings with a crystallite size of 26 and 15 nm, respectively.

 (v) Electrochemical pre-treatment of carbon substrate in 1 M KOH decreases the overpotential of HER and the Tafel slope for nickel coating to $-120$ mV and $-135$ mV·dec$^{-1}$.

## Appendix
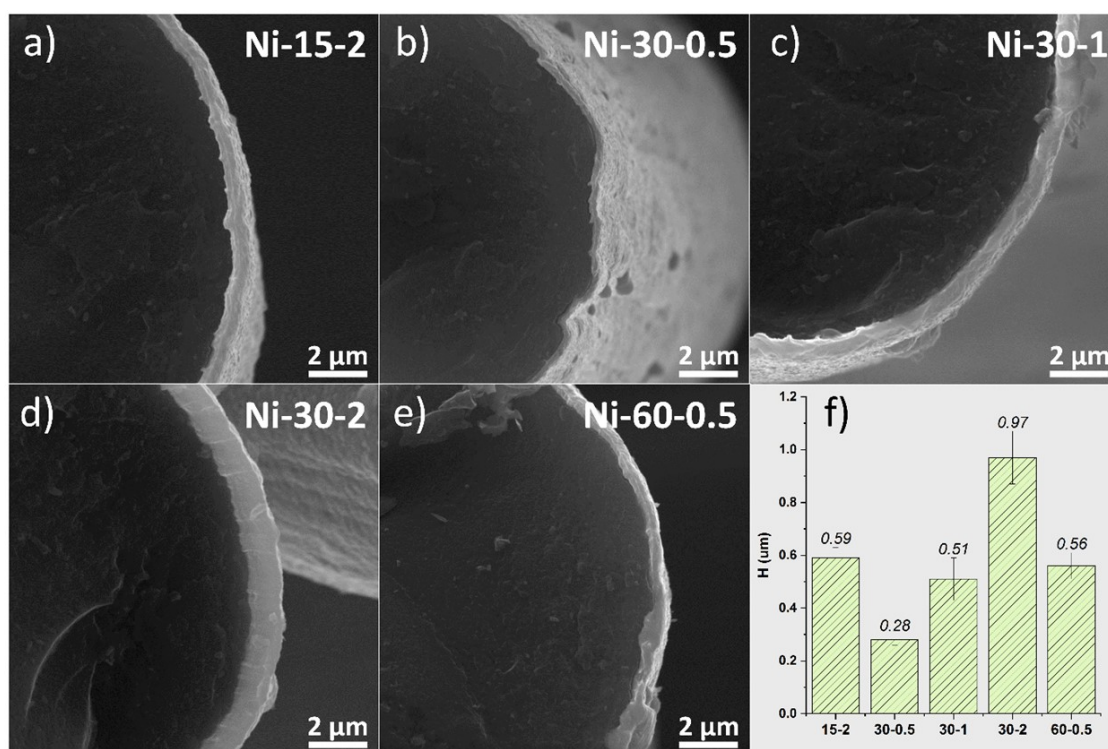


FIG. A1. SEM images of samples (a-e) and average coating thicknesses (e)
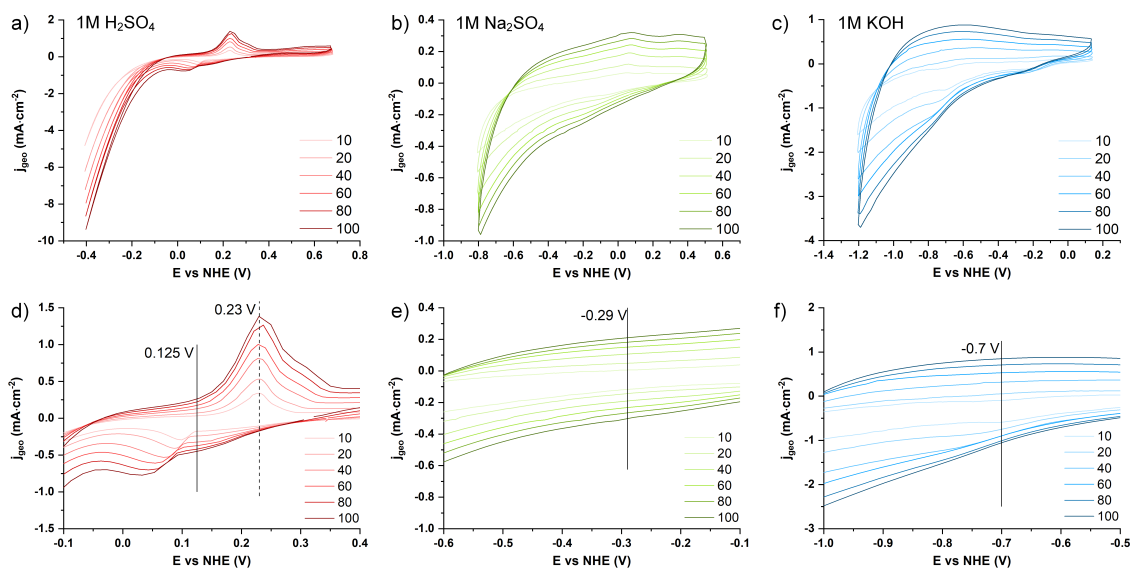
FIG. A2. CVA curves of carbon felt in 1 M $H_2SO_4$ (a,d), 1 M $Na_2SO_4$ (b,e), 1 M KOH (c,f)
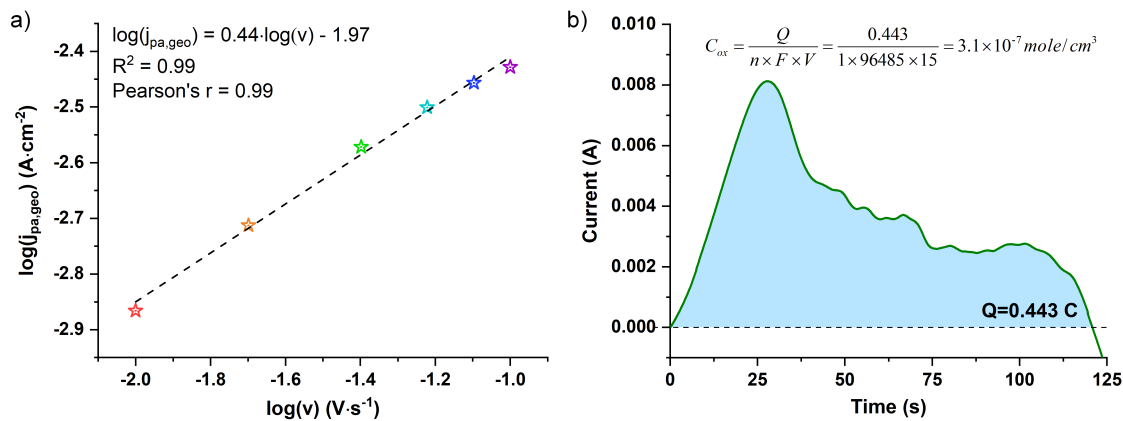


FIG. A3. Logarithmic plot (a) and $I - t$ graph of $[Fe(CN)_6]^{4-}/[Fe(CN)_6]^{3-}$ process ($v = 10$ mVs$^{-1}$)
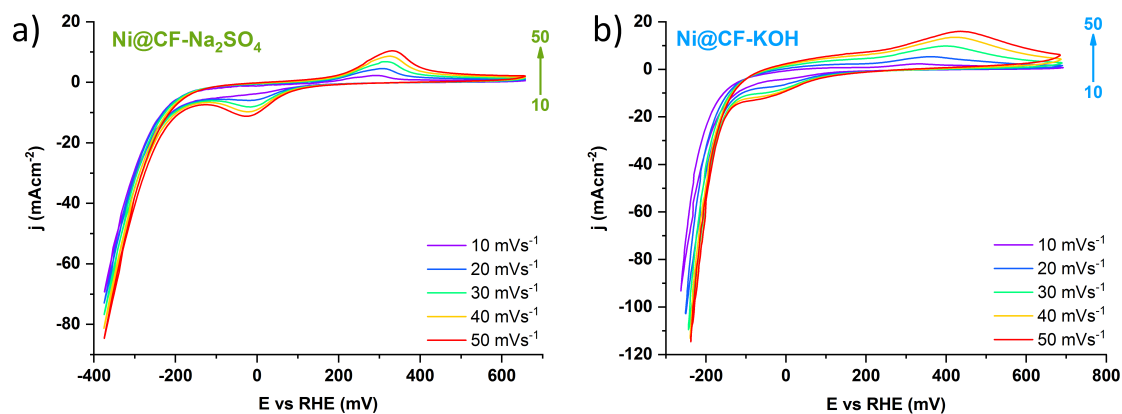


FIG. A4. CVA curves of Ni@CF-$Na_2SO_4$ (a) and Ni@CF-KOH (b)

## References

[1] Huong Le T.X., Bechelany M., Cretin M. Carbon felt based-electrodes for energy and environmental applications: A review. *Carbon N. Y.*, 2017, **122**, P. 564–591.

[2] Uan J.Y., Chen Y.J., Hsu Y.H., Arpornwichanop A., Chen Y.S. Deposition of Li/Al layered double hydroxides on the graphite felts for the performance improvement of an all-vanadium redox flow battery. *Mater. Today Commun.*, 2021, **27**, 102280.

[3] Kim M., Park J., Yeo G., Ko M., Jang H. Designing CNT-implanted graphite felt as a sustainable electron network for long-cycling of vanadium redox flow batteries. *Carbon N. Y.*, 2023, **206**, P. 1–6.

[4] Abbas S., Lee H., Hwang J., Mehmood A., Shin H.-J., Mehboob S., Lee J.Y., Ha H.Y. A novel approach for forming carbon nanorods on the surface of carbon felt electrode by catalytic etching for high-performance vanadium redox flow battery. *Carbon N. Y.*, 2018, **128**, P. 31–37.

[5] Moghim M.H., Eqra R., Babaiee M., Zarei-Jelyani M., Loghavi M.M. Role of reduced graphene oxide as nano-electrocatalyst in carbon felt electrode of vanadium redox flow battery. *J. Electroanal. Chem.*, 2017, **789**, P. 67–75.

[6] Anarghya D., Anantha M.S., Venkatesh K., Santosh M.S., Priya M.G., Muralidhara H.B. Bermuda grass derived nitrogen-doped carbon as electrocatalyst in graphite felt electrode to increase the efficiency of all-iron redox flow batteries. *J. Electroanal. Chem.*, 2020, **878**, 114577.

[7] León M.I., Arenas L.F., Walsh F.C., Nava J.L. Simulation of a vanadium-cerium redox flow battery incorporating graphite felt electrodes. *J. Electroanal. Chem.*, 2021, **903**, 115847.

[8] Jin C.-B., Shi P., Zhang X.-Q., Huang J.Q. Advances in carbon materials for stable lithium metal batteries. *New Carbon Mater.*, 2022, **37**, P. 1–24.

[9] Wang Y., Zhu M., Liu H., Zhang Y., Wu K., Wang G., Wu C. Carbon-based current collector materials for sodium metal anodes. *New Carbon Mater.*, 2022, **37**, P. 93–108.

[10] Zhang J., Wang W., Shi R., Wang W., Wang S., Kang F., Li B. Three-dimensional carbon felt host for stable sodium metal anode. *Carbon N. Y.*, 2019, **155**, P. 50–55.

[11] Watson V.G., Haynes Z.D., Telama W., Yeboah Y.D., Weatherspoon M.H., Zheng J.P., Kalu E.E. Electrochemical performance of heat treated $SnO_2$–SnCu@C-Felt anode materials for lithium ion batteries. *Surfaces and Interfaces*, 2018, **13**, P. 224–232.

[12] Gong Y., Xue Y. Carbon nanomaterials for stabilizing zinc anodes in zinc-ion batteries. *New Carbon Mater.*, 2023, **38**, P. 438–454.

[13] Wu M., Tian X., Yang W., Guo B., Guo J. Co nanoparticles embedded in wheat-like porous carbon nanofibers as bifunctional electrocatalysts for rechargeable zinc-air batteries. *Electrochim. Acta*, 2022, **411**, 140090.

[14] Chen W., Liu X., Wu J., Wang Q., Zhang Y., Yan S., Hou P., Luo S. Electrospun $Fe_{1-x}S@$ nitrogen-doped carbon fibers as anode material for sodium-ion batteries. *J. Electroanal. Chem.*, 2023, **929**, 117095.

[15] Peng J., Luo J., Li W., Zeng P., Wu Z., Wang Y., Li J., Shu H., Wang X. Insight into the performance of the mesoporous structure $SiO_x$ nanoparticles anchored on carbon fibers as anode material of lithium-ion batteries. *J. Electroanal. Chem.*, 2021, **880**, 114798.

[16] Wu M., Zhao X., Gao J., Guo J., Xiao J., Chen R. Multifunctional boron-doped carbon fiber electrodes synthesized by electrospinning for supercapacitors, dye-sensitized solar cells, and photocapacitors. *Surfaces and Interfaces*, 2022, **31**, 101983.

[17] Sawadsitang S., Duangchuen T., Karaphun A., Putjuso T., Kumnorkaew P., Swatsitang E. Synthesis, characterization and electrochemical properties of activated coconut fiber carbon (ACFC) and CuO/ACFC nanocomposites for applying as electrodes of supercapacitor devices. *Surfaces and Interfaces*, 2021, **25**, 101174.

[18] Ye D., Yu Y., Tang J., Liu L., Wu Y. Electrochemical activation of carbon cloth in aqueous inorganic salt solution for superior capacitive performance. *Nanoscale*, 2016, **8**, P. 10406–10414.

[19] Rodrigues A.C., da Silva E.L., Oliveira A.P.S., Matsushima J.T., Cuña A., Marcuzzo J.S., Gonçalves E.S., Baldan M.R. High-performance supercapacitor electrode based on activated carbon fiber felt/iron oxides. *Mater. Today Commun.*, 2019, **21**, 100553.

[20] Wang S., Liu Y., Wang Q., Liu P., Li L., Wang T. Fabrication of self-doped aramid-based porous carbon fibers for the high-performance supercapacitors. J. Electroanal. Chem., 2022, 923, P. 116829.

[21] Zhang L., Yu X., Zhu P., Sun R., Wong C. Surface functional treatment of carbon fiber with ultra wide potential range in neutral electrolyte for high performance supercapacitor. *J. Electroanal. Chem.*, 2020, 876, 114478.

[22] Toyoda M., Inagaki M. Carbon materials for solar steam-generation. *Carbon N. Y.*, 2023, **214**, 118373.

[23] Hidalgo D., Tommasi T., Bocchini S., Chiolerio A., Chiodoni A., Mazzarino I., Ruggeri B. Surface modification of commercial carbon felt used as anode for Microbial Fuel Cells. *Energy*, 2016, **99**, P. 193–201.

[24] Zhuang H., Yang F. Vanadium metal-organic framework derived 2D hierarchical VO2 nanosheets grown on carbon cloth for advanced flexible energy storage devices. *Surfaces and Interfaces*, 2021, **25**, 101232.

[25] Xu H., Zhang M., Ma Z., Zhao N., Zhang K., Song H., Li X. Improving electron transport efficiency and power density by continuous carbon fibers as anode in the microbial fuel cell. *J. Electroanal. Chem.*, 2020, **857**, 113743.

[26] Chen S., Tang L., Feng H., Zhou Y., Zeng G., Lu Y., Yu J., Ren X., Peng B., Liu X. Carbon felt cathodes for electro-Fenton process to remove tetracycline via synergistic adsorption and degradation. *Sci. Total Environ.*, 2019, **670**, P. 921–931.

[27] Koca M.B., Gümüşgöz Çelik G., Kardaş G., Yazıcı B. NiGa modified carbon-felt cathode for hydrogen production. *Int. J. Hydrogen Energy*, 2019, P. 14157–14163.

[28] Fan X., Ma Y., Sun A., Zhang X., Tang L., Guo J. Engineering heterogeneous nickel-iron oxide/iron phosphate on P, N co-doped carbon fibers for efficient oxygen evolution reaction in neutral and alkaline solutions. *Surfaces and Interfaces*, 2021, **25**, 101193.

[29] Jin Y., Zhang T., Pan N., Wang S., Zhang B., Zhu X., Hao Y., Wang X., Song L., Zhang M. Surface functionalization of carbon cloth with conductive Ni/Fe-MOFs for highly efficient oxygen evolution. *Surfaces and Interfaces*, 2022, **33**, 102294.

[30] Lee D.J., Kumar G.M., Sekar S., Ganesh V., Jeon H.C., Kim D.Y., Kang T.W., Ilanchezhiyan P. $Re_{1-x}Ni_xS_2$ nanosheets for high efficient electrocatalytic hydrogen evolution functions. *Surfaces and Interfaces*, 2023, **40**, 103014.

[31] Dmitriev D.S., Tenevich M.I. Electrocatalytic performance of nickel coating on carbon felt with silver particles inclusions. *J. Taiwan Inst. Chem. Eng.*, 2022, **141**, 104591.

[32] Ifires M., Addad A., Barras A., Hadjersi T., Chegroune R., Szunerits S., Boukherroub R., Amin M.A. Cathodic pre-polarization studies on the carbon felt/KOH interface: An efficient metal-free electrocatalyst for hydrogen generation. *Electrochim. Acta*, 2021, **375**, 137981.

[33] García-Rodríguez O., Banuelos J.A., El-Ghenymy A., Godínez L.A., Brillas E., Rodríguez-Valadez F.J. Use of a carbon felt–iron oxide air-diffusion cathode for the mineralization of Malachite Green dye by heterogeneous electro-Fenton and UVA photoelectro-Fenton processes. *J. Electroanal. Chem.*, 2016, **767**, P. 40–48.

[34] Liu L., Zhang D., Duan D., Li Y., Yuan Q., Chen L., Liu S. In situ fabrication of 3D self-supporting cobalt phosphate-modified graphite felt electrocatalysts for oxygen evolution reaction in neutral solution. *J. Electroanal. Chem.*, 2020, **862**, 114031.

[35] Zhang G., Yu J., Su C., Di C., Ci S., Mou Y., Fu Y., Qiao K. The effect of annealing on the properties of copper-coated carbon fiber. *Surfaces and Interfaces*, 2023, **37**, 102630.

[36] Dmitriev D.S., Martinson K.D., Popkov V.I. Electrochemical template synthesis of copper hollow microtubes with dendritic surface and advanced HER performance. *Mater. Lett.*, 2021, **305**, 130808.

[37] Zhou Q., Li G., Qu Y., Zhou S., Xu W., Gao X., Yang F., Li R. Preparation and antioxidation of Cu–Sn composite coating on the surface of Cu-coated carbon fibers. *Surfaces and Interfaces*, 2022, **31**, 102016.

[38] Jakóbczyk P., Skowierzak G., Kaczmarzyk I., Nadolska M., Wcislo A., Lota K., Bogdanowicz R., Ossowski T., Rostkowski P., Lota G., Ryl J. Electrocatalytic performance of oxygen-activated carbon fibre felt anodes mediating degradation mechanism of acetaminophen in aqueous environments. *Chemosphere*, 2022, **304**, 135381.

[39] Dmitriev D.S., Tenevich M.I., Lobinsky A.A., Popkov V.I. Coaxial structures based on NiO/Ni@Carbon felt: Synthesis features, electrochemical behavior and application perspectives. *J. Electroanal. Chem.*, 2022, **911**, 116216.

[40] Zhou H., Zhang H., Zhao P., Yi B. A comparative study of carbon felt and activated carbon based electrodes for sodium polysulfide/bromine redox flow battery. *Electrochim. Acta*, 2006, **51**, P. 6304–6312.

[41] Jing M., Xu Z., Fang D., Fan X., Liu J., Yan C. Improvement of the Battery Performance of Vanadium Flow Battery by Enhancing the Specific Surface Area of the Carbon Felt Electrodes: II. Digging Effect. *J. Electrochem. Soc.*, 2021, **168**, 030539.

[42] Su Y., Chen N., Ren H., Guo L., Li Z., Wang X. Preparation and Properties of Indium Ion Modified Graphite Felt Composite Electrode. *Front. Chem.*, 2022, **10**, P. 1–7.

[43] Popat Y., Trudgeon D., Zhang C., Walsh F.C., Connor P., Li X. Carbon Materials as Positive Electrodes in Bromine-Based Flow Batteries. *Chempluschem*, 2022, **87**.

[44] Jiang H.R., Shyy W., Wu M.C., Zhang R.H., Zhao T.S. A bi-porous graphite felt electrode with enhanced surface area and catalytic activity for vanadium redox flow batteries. *Appl. Energy*, 2019, **233–234**, P. 105–113.

[45] Gautam R.K., Kapoor M., Verma A. Tactical Surface Modification of a 3D Graphite Felt as an Electrode of Vanadium Redox Flow Batteries with Enhanced Electrolyte Utilization and Fast Reaction Kinetics. *Energy & Fuels*, 2020, **34**, P. 5060–5071.

[46] Noh T.H., Kim M.Y., Kim D.H., Yang S.H., Lee J.H., Park H.S., Noh H.S., Lee M.S., Kim H.S. Electrochemical studies of carbon felt electrode modified under airless conditions for redox flow batteries. *J. Electrochem. Sci. Technol.*, 2017, **8**, P. 155–161.

[47] Zhou X., Zhang X., Lv Y., Lin L., Wu Q. Nano-catalytic layer engraved carbon felt via copper oxide etching for vanadium redox flow batteries. *Carbon N. Y.*, 2019, **153**, P. 674–681.

[48] González-García J., Bonete P., Expósito E., Montiel V., Aldaz A., Torregrosa-Maciá R. Characterization of a carbon felt electrode: structural and physical properties. *J. Mater. Chem.*, 1999, **9**, P. 419–426.

[49] Wang Y., Lin B. Enhancement of performance for graphite felt modified with carbon nanotubes activated by KOH as Cathode in electro-fenton systems. *J. Appl. Biomater. Funct. Mater.*, 2021, **19**, 228080002110053.

[50] Rabbow T.J., Whitehead A.H. Deconvolution of electrochemical double layer capacitance between fractions of active and total surface area of graphite felts. *Carbon N. Y.*, 2017, **111**, P. 782–788.

[51] Kato K., Kano K., Ikeda T. Electrochemical Characterization of Carbon Felt Electrodes for Bulk Electrolysis and for Biocatalyst-Assisted Electrolysis. *J. Electrochem. Soc.*, 2000, **147**, 1449.

*Information about the authors:*

*Dmitry S. Dmitriev* – Ioffe Institute, 194021 Saint Petersburg, 26 Polytechnicheskaya street, Russian Federation; ORCID 0000-0002-7261-6694; elchemorg@gmail.com

*Maksim I. Tenevich* – Ioffe Institute, 194021 Saint Petersburg, 26 Polytechnicheskaya street, Russian Federation; ORCID 0000-0003-2003-0672; chwm420@gmail.com

*Conflict of interest*: the authors declare no conflict of interest.